VOL. 16, NO. 23, DECEMBER 2021 ISSN 1819-6608
ARPN Journal of Engineering and Applied Sciences

www.arpnjournals.com

A COMPARISON OF VEHICLE RIDE COMFORT PERFORMANCE OF HYDRAULIC ENGINE MOUNT SYSTEM WITH RUBBER ENGINE MOUNT SYSTEM

Ta Tuan Hung[1], Le Van Quynh[2], Dang Viet Ha[3], Canh Chi Huan[2], Bui Van Cuong[2] and Hoang Anh Tan[2]
[1]Faculty of Mechanical Engineering, University of Transport Technology, Hanoi, Vietnam
[2]Faculty of Automotive and Power Machinery Engineering, Thai Nguyen University of Technology, Thai Nguyen, Vietnam
[3]Vietnam Register, Ha Noi, Viet Nam
E-Mail: lequynh@tnut.edu.vn

ABSTRACT

In order to assess the vehicle ride comfort performance between the hydraulic engine mount system (HEMs) and rubber engine mount system (REMs), both dynamic models of the hydraulic engine mount (HEM) with inertia track and decoupler and the rubber engine mount (REM) are established to determine the vertical forces. And then the vertical forces of engine mounts are linked with a full-vehicle dynamic model under the combination of two excitation sources such as internal combustion engine and road surface excitations. The time domain root mean square (r.m.s) and power spectral density (PSD) acceleration responses of the vertical motion, pitch and roll angles of vehicle body are chosen as objective functions to compare the vehicle ride comfort performance of the two engine mounts. The study results show that the values of the root mean square (r.m.s) acceleration responses with HEMs are respectively reduced in comparison with REMs and the peak values of PSD acceleration responses are respectively reduced when compared with REMs in low frequency region from 0.5Hz to 10Hz when both the vehicle and engine operate under the different operating conditions. Vehicle ride comfort is significantly improved with HEMs in low frequency region.

Keywords: internal combustion engine (ICE), Hydraulic engine mount (HEM), rubber engine mount (REM), dynamic model, ride comfort.

1. INTRODUCTION

Vehicle engine mount has an important role in reducing the sources of engine vibrations transmitting to the vehicle body and vehicle body vibrations transmitting to the engine. It is also used to improve vehicle ride comfort and reduce vehicle noise. The optimal designs for vehicle engine mounts have been an interesting topic for researchers in all over the world. An optimal design of rubber engine mount (REM) was proposed with the objective functions such as the weight and the maximum stress using a microgenetic algorithm (MGA) [1]. The engine rubber mount (REM) was proposed and considered for the optimal design in many different ways such as a density based topology optimization method [2], a multi-objective optimization model [3], ANSYS optimization design [4] and TRIZ-Morphological chart-analytic network process technique [5]. One of the limitations of REM is the small damping coefficient that is difficult to reduce vibrations at low excitation frequencies. For this reason, hydraulic engine mounting (HEM) was proposed and replaced the rubber engine mount (ERM). The optimum values of mass and damping of the fluid in the orifice of HEM were found out by a design optimization theory for a conventional dynamic absorber [6]. A new HEM design using two working fluids was suggested [7]. The optimal design methods for HEMS using a genetic neural network (NN) algorithm [8] and RMS averaging of the frequency response functions [9] were presented to improve their performance. To improve vehicle ride comfort quality and reduce vehicle noises through control algorithms, a new hydraulic engine mount was proposed with a controllable area of inertia track [10]. A semi-active hydraulic engine mount was improved into a passive hydraulic engine mount which used a novel auxiliary magnetorheological (MR) fluid chamber [11]. A mixed mode-type magneto-rheological fluid mount was developed by considering the nondimensional formulation of Bingham plastic flow [12]. The full-vehicle dynamic models including engine, vehicle body and axle masses were proposed to evaluate and analyze the effects of engine vibrations and characteristics of engine mounting system on vehicle ride comfort. The characteristics of vehicle engine mounting system such REMs with the hydraulic actuator [13], HEMs with regard to the inertia and resistance of the fluid within the inertia track[15], and semi-active electro-rheological (ER) engine mounts[15] were analyzed and evaluated their effects on vehicle ride comfort when a full – vehicle dynamic model is used. Three different types of engine mount systems including REMs, HEMs and semi-active engine mounts (SEMs) were proposed to compare the vehicle's ride performance when a full - vehicle dynamic model is used [16].

The primary goal of the study is to compare the ride comfort performance of hydraulic engine mount system (HEMs) with that of rubber engine mount system (REMs). Both non-linear and linear dynamic model of the hydraulic engine mount (HEM) with inertia track and decoupler and the rubber engine mount (REM) are established to determine the vertical forces. And then, the vertical forces of engine mounts are linked with a full-vehicle dynamic model under the combination of two excitation sources. The ride comfort performance of HEMs is respectively analyzed through the objective functions based to the ISO 2631:1997(E) standard [27].

VOL. 16, NO. 23, DECEMBER 2021 ISSN 1819-6608
ARPN Journal of Engineering and Applied Sciences

2. VEHICLE AND ENGINE DYNAMIC MODEL

2.1 Non-Linear Dynamic Model of HEM

The optimal designs for the engine mounts are constantly evolving in the direction of reducing engine noises and vibrations. The passive hydraulic engine mounts are widely used in automotive engines, and they compose of two main parts- rubber parts and hydraulic actuators. The hydraulic actuator is a component that changes the hydraulic damping coefficient by the inertia of the fluid flows circulating through the valve holes of two fluid chambers. According to the recommendations of most of the literatures [17-23], a passive hydraulic engine mounts with inertia track and decoupler chosen for the analytical study is illustrated in Figure-1. Based on the schematic of Figure-1 and the interactions between fluids and mechanical structures, a lumped parameter system model of a passive hydraulic engine mount, as in Figure-2, is established when the stiffness and damping coefficient of the rubber part of engine mount are kr and cr respectively; the fluid compliances of upper and lower chambers are C_1 and C_2 respectively; the effective pumping area is A_p; the effective inertia and resistance of decoupler are I_d and R_d respectively; The inertia and resistance of inertia track are I_i and R_i respectively; The volumetric flow rates through the inertia track and decoupler are $q_i(t)$ and $q_d(t)$ respectively; The upper and lower chamber pressures are $p_1(t)$ and $p_2(t)$ respectively; The vehicle body and engine masses are m_b and m_e respectively; The vertical displacements of vehicle body and engine are z_b and z_e respectively; The vertical forces of HEMs is F_{h1} and F_{h2}.

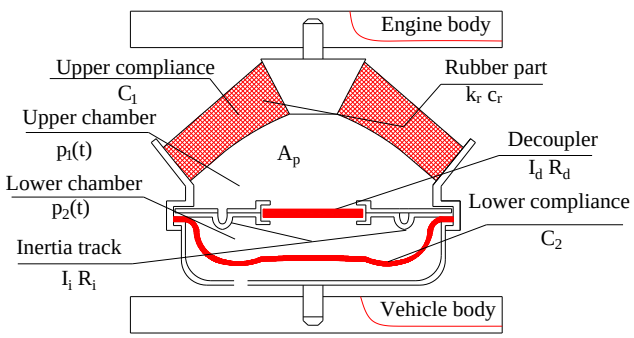

Figure-1. A schematic of a hydraulic engine mount with inertia track and decoupler.

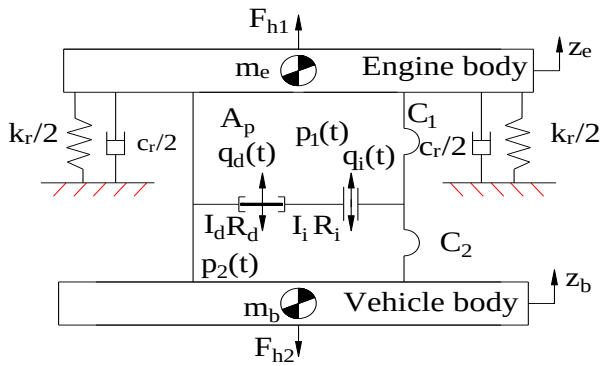

Figure-2. Lumped parameter system model of a hydraulic engine mount with inertia track and decoupler.

The dynamic equations of hydraulic actuators shown in Figure-2 can be derived considering the continuity and momentum equations from the references [17-23]. The continuity equations of the fluid in upper and lower chambers are defined below:

$$\begin{cases} A_p\left(\dot{z}_e-\dot{z}_b\right)-q_i(t)-q_d(t)=C_1\dot{p}_1(t) \\ q_i(t)+q_d(t)=C_2\dot{p}_2(t) \end{cases} \quad (1)$$

The momentum equations of the fluid in the inertia track and decoupler are defined below:

$$\begin{cases} p_1(t)-p_2(t)=I_i\dot{q}_i+R_i\dot{q}_i & \text{if decoupler is contacting the cage} \\ p_1(t)-p_2(t)=I_d\dot{q}_d+R_d\dot{q}_d & \text{if the decoupler is free} \end{cases} \quad (2)$$

Under the dynamic excitation (z_e-z_b), the transmitted force F_{e2} is obtained from the references [20, 23]

$$\begin{cases} F_{e2}=k_r\left(z_e-z_b\right)+c_r\left(\dot{z}_e-\dot{z}_b\right)+A_p\left(p_1(t)-p_2(t)\right)+A_p p_2(t) & \text{if decoupler is contacting the cage} \\ F_{e2}=k_r\left(z_e-z_b\right)+c_r\left(\dot{z}_e-\dot{z}_b\right)+\left(A_p-A_p\right)+A_p p_2(t)+A_d R_d q_d(t) & \text{if the decoupler is free} \end{cases} \quad (3)$$

To facilitate the analysis in this study, the approximate model of the hydraulic mount with inertia track and decoupler is established based on the literatures [21, 22], as shown Figure-3. The model effective values include the inertia track fluid mass $m_i=A_p^2I_i$, the decoupler fluid mass $m_d=A_p^2I_d$, the inertia track damping $c_{hi}= A_p^2R_i$, the decoupler damping $c_{hd}= A_p^2R_d$, the upper chamber fluid stiffness $k_{h1}= A_p^2/C_1$, the lower chamber fluid stiffness $k_{h2}= A_p^2/C_2$, The absolute displacement of the inertia track fluid mass (m_i) z_{hi}, and the the relative displacement between the effective masses (m_i and m_d) z_{hd}.

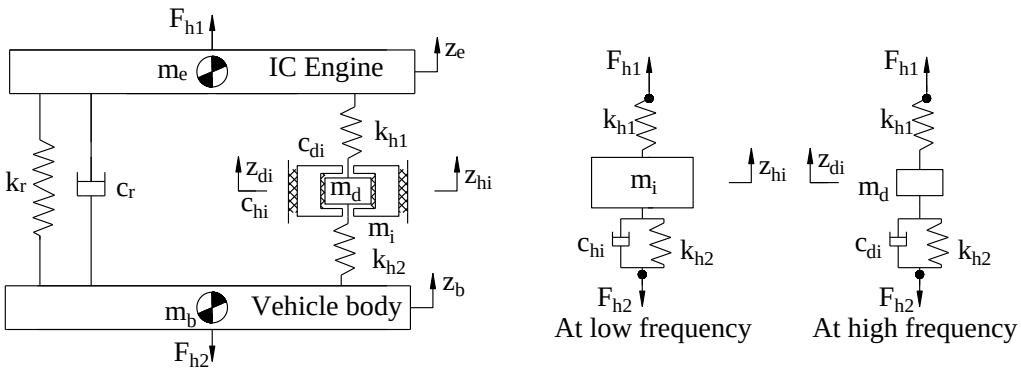

Figure-3. Approximate model of the hydraulic engine mount with inertia track and decoupler.

The vertical forces of HEM with inertia track and decoupler transmitting to the engine and vehicle bodies are considered in two cases below.

Case 1: The decoupler is contacting the cage in which HEM is only considered as an inertia track fluid mass element at low frequencies, $q_d(t)\approx 0$, $R_d\rightarrow\infty$. The vertical forces of HEM transmitting to engine and vehicle bodies [22] are defined as:

$$\begin{cases} F_{e1} = F_r + F_{h1} = k_r(z_e - z_b) + c_r(\dot{z}_e - \dot{z}_b) + k_{h1}(z_e - z_{hi}) \\ F_{e2} = F_r + F_{h2} = k_r(z_e - z_b) + c_r(\dot{z}_e - \dot{z}_b) + k_{h2}(z_{hi} - z_b) + c_{hi}(\dot{z}_{hi} - \dot{z}_b) \end{cases} \quad (4)$$

The effective governing equation of the inertia track fluid mass m_i is defined as:

$$m_i\ddot{z}_{hi} = k_{h1}(z_e - z_{hi}) - k_{h2}(z_{hi} - z_b) - c_{hi}(\dot{z}_{hi} - \dot{z}_b) \quad (5)$$

Case 2: The decoupler is free and HEM is considered as a decoupler fluid mass element at high frequencies, $q_i(t)\approx 0$, $R_i\rightarrow\infty$. The vertical forces of HEM transmitted to engine and vehicle bodies [22] are defined as:

$$\begin{cases} F_{e1} = F_r + F_{h1} = k_r(z_e - z_b) + c_r(\dot{z}_e - \dot{z}_b) + k_{h1}(z_e - z_{di}) \\ F_{e2} = F_r + F_{h2} = k_r(z_e - z_b) + c_r(\dot{z}_e - \dot{z}_b) + k_{h2}(z_{di} - z_b) + c_{di}(\dot{z}_{di} - \dot{z}_b) \end{cases} \quad (6)$$

The effective governing equation of the decoupler fluid mass m_d is defined as:

$$m_d\ddot{z}_{di} = k_{h1}(z_e - z_{di}) - k_{h2}(z_{di} - z_b) - c_{di}(\dot{z}_{di} - \dot{z}_b) \quad (7)$$

2.2 Linear Dynamic Model of REM

The traditional rubber engine mount is commonly used to reduce vibrations in high frequencies and the dynamic model of rubber engine mount is shown in Figure-4.

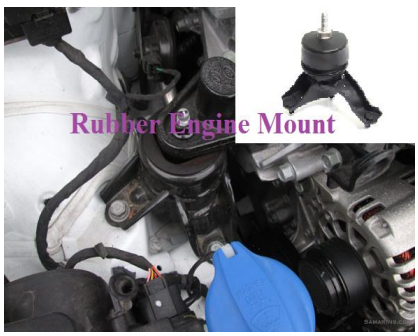

(a) Rubber engine mount

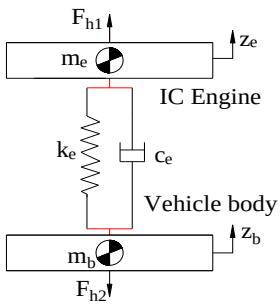

(b) Lumped parameter system model of REM

Figure-4. Dynamic model of rubber engine mount.

From Figure-4(a), the vertical forces of REM transmitting to engine and vehicle bodies [22] are defined as:

$$F_{h1} = F_{h2} = k_e(z_e - z_b) + c_e(\dot{z}_e - \dot{z}_b) \quad (8)$$

2.3 Full-Vehicle Dynamic Model

To evaluate the vehicle ride comfort performance of the hydraulic engine mount system, a 3-D vehicle dynamic model including engine, vehicle body and axle masses with 10 degrees of freedom (DOFs) is set up to analyze the quality of an optimal controller for a semi-active hydraulic engine mount, as shown in Figure-5.

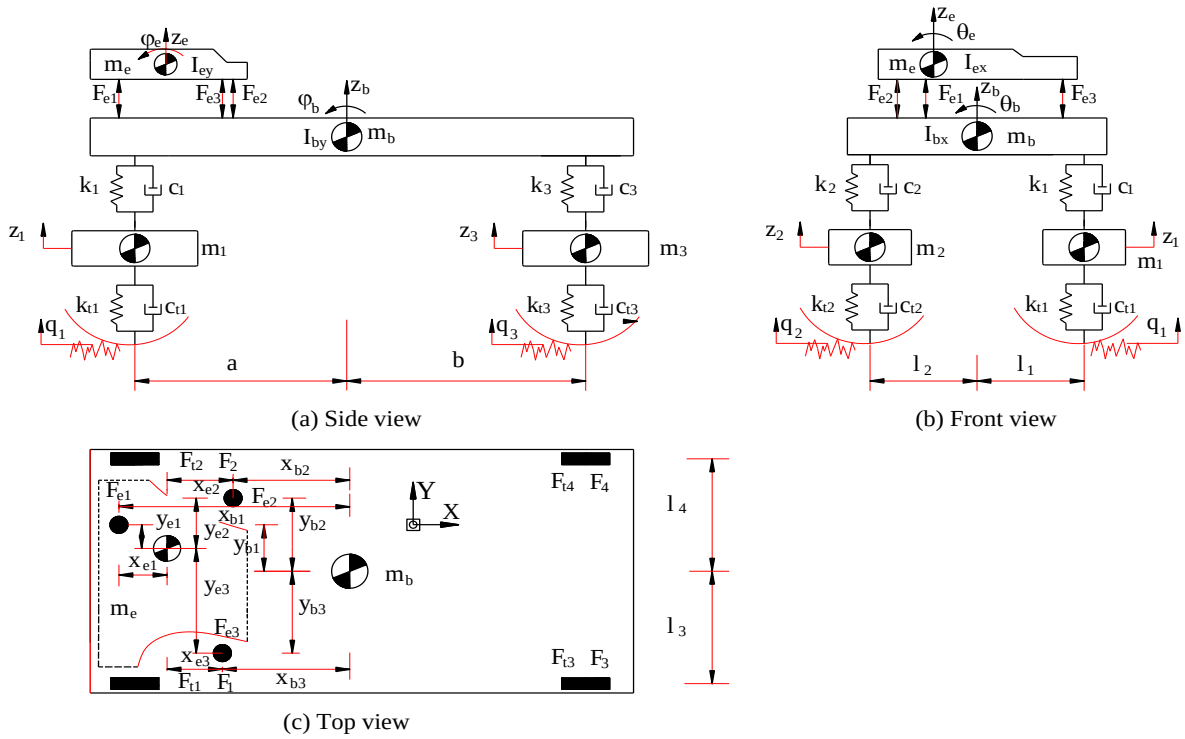

Figure-5. A 3-D full- vehicle dynamic model.

Explanation of the symbols for Figure-5, the vertical displacements of engine body, vehicle body, and axles are m_e, m_b, and m_s, the angular and vertical displacements are z_e, z_b, and z_s, the angular displacements of engine and vehicle bodies are φ_e, θ_e and φ_b, θ_b, the inertia moments of engine and vehicle masses are I_{ex}, I_{ey} and I_{bx}, I_{by}, the stiffness and damping coefficients of vehicle suspension systems, engine mounting systems and tires are k_{en}, and c_{en}, k_s and c_s and k_{ts} and c_{ts}, the distances are a, b and l_s, X and Y-position of engine mount No.1, No.2 and No.3 with respect to the center of gravity of the vehicle body are x_{bn} and y_{bn}; X and Y-position of engine mount No.1, No.2 and No.3 with respect to the center of gravity of the engine body are x_{en} and y_{en} and the road surface excitations are denoted by q_n (s=1÷4, n=1÷3).

In this study, a combined method of the multi-body system theory and D'Alembert's principle is chosen. The multi-body system theory is used to separate the system into subsystems which are linked by the force and moment equations. D'Alembert's principle is used to make up force and moment equations to describe vehicle dynamic subsystems. The equations of motion of objects in Figure-5 can be written by a combined method as follows.

The equations of motion for the vertical, pitch and roll motions of engine body are written as follows:

$$\begin{cases} m_e\ddot{z}_e = F_{ez} - \sum_{n=1}^{n=3} F_{h1n} \\ I_{ey}\ddot{\varphi}_e = M_{ey} + F_{h11}x_{e1} - F_{h12}x_{e2} - F_{h13}x_{e3} \\ I_{ex}\ddot{\theta}_e = M_{ex} + F_{h11}y_{e1} + F_{h12}y_{e2} - F_{h13}y_{e3} \end{cases} \tag{9}$$

where,

$$F_{h1n} = k_{rn}(z_{e0n} - z_{b0n}) + c_{rn}(\dot{z}_{e0n} - \dot{z}_{b0n}) + k_{h1n}(z_{e0n} - z_{hn}),$$

$$k_{h1n} = \begin{cases} A_{pn}^{\ 2}/C_{1n} & \text{At low excitation frequencies} \\ A_{pn}^{\ 2}/C_{2n} & \text{At high excitation frequencies} \end{cases},$$

$$z_{hn} = \begin{cases} z_{hin} & \text{At low excitation frequencies} \\ z_{hdn} & \text{At high excitation frequencies} \end{cases}$$

n=1÷3, $z_{e01} = z_e - x_{e1}\varphi_e - y_{e1}\theta_e$,

$z_{e02} = z_e + x_{e2}\varphi_e - y_{e2}\theta_e$, $z_{e03} = z_e + x_{e3}\varphi_e + y_{e3}\theta_e$.

The equations of motion for the vertical, pitch and roll motions of vehicle body are written as follows:

$$\begin{cases} m_b\ddot{z}_b = \sum_{n=1}^{n=3} F_{h2n} - \sum_{s=1}^{s=4} F_s \\ I_{bx}\ddot{\varphi}_b = \sum_{s=1}^{s=2} F_s l_1 - \sum_{s=3}^{s=4} F_s l_2 - F_{h21}x_{b1} - F_{h22}x_{b2} - F_{h23}x_{b3} \\ I_b\ddot{\theta}_b = \sum_{s=2}^{s=4} F_s l_3 - (F_1 + F_3)l_4 - F_{h21}y_{b1} - F_{h22}y_{b2} - F_{h23}x_{b3} \end{cases} \tag{10}$$

where,

$$F_{h2n} = k_{rn}(z_{e0n} - z_{b0n}) + c_{rs}(\dot{z}_{e0n} - \dot{z}_{b0n}) + k_{h2n}(z_{hn} - z_{b0n}) + c_{hn}(\dot{z}_{hn} - \dot{z}_{b0n})$$

$$k_{h2n} = \begin{cases} A_{pn}^{\ 2}/C_{1n} & \text{At low excitation frequencies} \\ A_{pn}^{\ 2}/C_{2n} & \text{At high excitation frequencies} \end{cases}$$

$$c_{hn} = \begin{cases} A_p^{\,2} R_{in} & \text{At low excitation frequencies} \\ A_p^{\,2} R_{dn} & \text{At high excitation frequencies} \end{cases}$$

n=1÷3,

$$z_{b01} = z_b - x_{b1}\varphi_b - y_{b1}\theta_b,\ z_{b02} = z_b - x_{b2}\varphi_b - y_{b2}\theta_b,$$

$$z_{b03} = z_b - x_{b3}\varphi_b + y_{b3}\theta_b\ F_s = k_s(z_{bs} - z_s) + c_s(\dot{z}_{bs} - \dot{z}_s)$$

$$z_{b1} = z_b - a\varphi_b + l_1\theta_b,\ z_{b2} = z_b - a\varphi_b - l_2\theta_b,$$

$$z_{b3} = z_b + b\varphi_b + l_3\theta_b,\ z_{b4} = z_b + b\varphi_b - l_4\theta_b.$$

The equations of motion for the vertical motions of vehicle body are written as follows:

$$m_s\ddot{z}_s = \sum_{s=1}^{s=4} F_s - \sum_{s=1}^{s=4} F_{ts} \tag{11}$$

where,

$$F_{ts} = k_{ts}(z_s - q_s) + c_{ts}(\dot{z}_s - \dot{q}_s)$$

3. ANALYSIS OF VIBRATION EXCITATION SOURCES ON VEHICLE BODY

Road surface excitation: The harmonic superposition method, filtering white noise method, AR method and ARMR model method are commonly used to describe the road surface roughness in time domain and frequency domain. In this study, the filtering white noise method is used to describe the time domain excitation of the road surface [16, 24] and time domain representation of the road surface can be given:

$$\dot{q}(t) + 2\pi f_0 q(t) = 2\pi n_0 \sqrt{G_q(n_0) v} w(t). \tag{12}$$

where, $G_q(n_0)$ is the road roughness coefficient which is defined for typical road classes from A (very good) to H (very poor) according to ISO 8068(1995) [25], v=f/n is the speed of vehicle from 10 m/s to 30 m/s, n is the road space frequency from 0.013 m^{-1} to 3.33 m^{-1}, and it can guarantee the temporal frequency of road surface f ranges from 0.33 Hz to 28.3 Hz which is the low excitation frequencies of road surface transmitted to vehicle body; f_0 is a minimal boundary frequency with a value of 0.0628 Hz; n_0 is a reference spatial frequency which is equal to 0.1 m; w(t) is a white noise signal. Matlab/Simulink software can be used to solve the process described by Eq. (13) to generate random road excitation and the results of the random road surface roughness time domain signal from ISO class A ($G_q(n_0)$ = 16/10^{-6} m^3) to ISO class D ($G_q(n_0)$ = 1024/10^{-6} m^3) at the vehicle speed of 20 m/s are shown Figure-6.

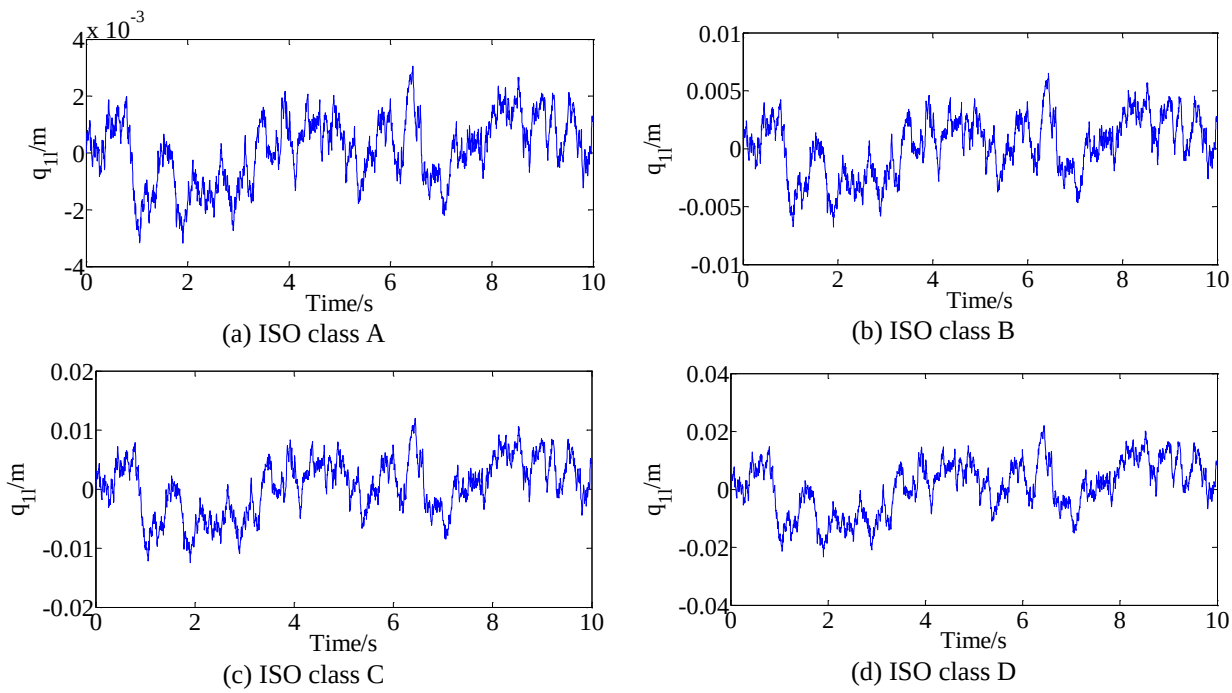

Figure-6. Random road surface roughness time domain signal according to the standard ISO 8068.

Internal combustion engine excitations: ICE vibration excitations transmitting to vehicle body are usually in the high excitation frequency range of 25-200 Hz with amplitudes generally less than 0.3 mm [23]. In this study, the vertical inertia excitation force due to the reciprocating mass of engine, the roll and pitch excitation moments of engine with a 4-stroke in-line engine [13, 15, 16, 26] are defined as:

$$F_{ez} = 4m_p r\lambda\omega^2 \cos(2\omega t) = 4m_p r\lambda\omega^2 \cos(2\pi ft) \quad (14)$$

$$M_{ex} = M_e\left[1+1.3\sin(2\omega t)\right] = M_e\left[1+1.3\sin(2\pi ft)\right] \quad (15)$$

$$M_{ey} = 4m_p r\lambda\omega^2 l_r \cos(2\omega t) = 4m_p r\lambda\omega^2 l_r \cos(2\pi ft) \quad (16)$$

where, $\omega=2\pi f$ is the angular velocity of crank shaft, $f= n_e/60$ is the excitation engine frequency, n_e is the engine speed, m_p is the piston mass, M_e is mean value of ICE torque $M_e= -6.810^{-6}n_e^2 + 0.059n_e + 112.5$ N.m, r is the rotational radius of crank arm, λ is the ratio of r to the length of the shaft, l_r is the distance between the CG and the centre-line of the second and third cylinders.

The vertical inertia excitation force due to the reciprocating mass of engine Eq.(14), the roll and pitch excitation moments of engine Eq.(15) and Eq.(16) are simulated by Matlab/Simulink software and the simulation results with mp=0.702kg, r=0.044m, λ=0.29, l_r= 0.135m, n_e=760rpm [15] are shown Figure-7.

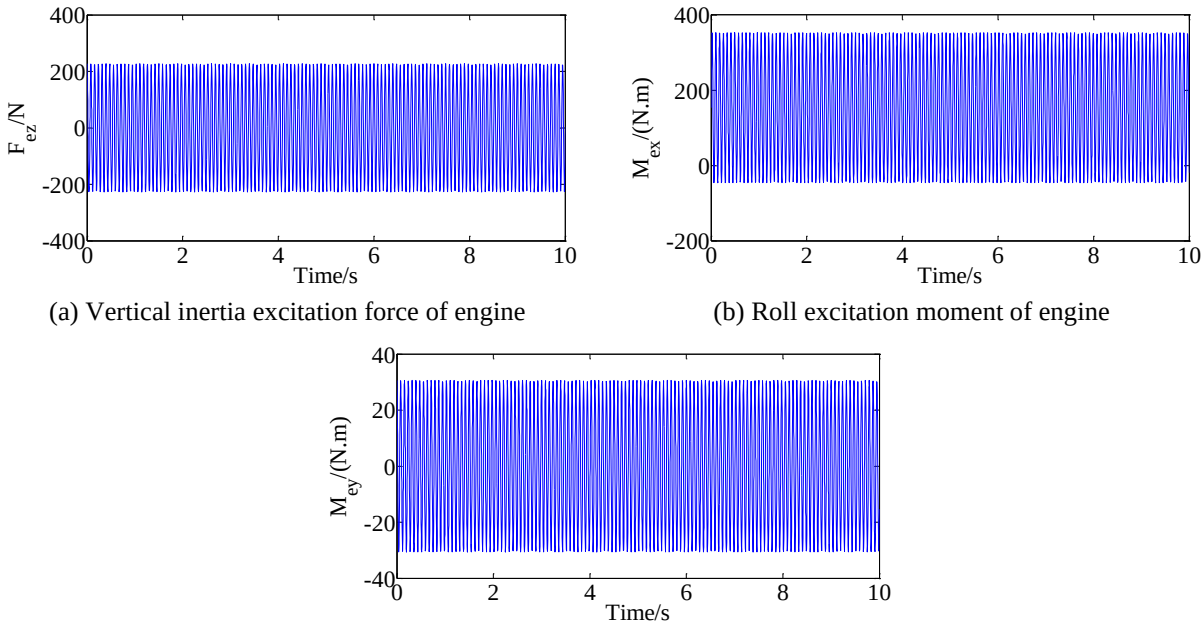

(a) Vertical inertia excitation force of engine

(b) Roll excitation moment of engine

(c) Pitch excitation moment of engine

Figure-7. Vertical inertia excitation force, roll and pitch excitation moments of engine.

4. RESULTS AND ANALYSIS

In order to analyze and compare the ride comfort performance of hydraulic engine mount system (HEMs) with that of rubber engine mount system (REMs), Matlab/simulink software is used to solve the equations of motion in the above section with vehicle and engine parameters in Table-1 and Table-2 when the vehicle and engine operate under different road conditions. The simulation results of the time domain acceleration responses of the vertical motion (a_b), pitch and roll angles (a_{phi} and a_{teta}) of vehicle body are shown in Figure-8 when the vehicle moves on ISO class B surfaces road condition and ICE engine operates at the speed of 1400 rpm (v≈60km/h at i_{h5}=0.775). The relationship between the speed of the vehicle and engine and the manual transmission system (MTs) is determined by Eq. (17).

$$v = 0.377\frac{r_b n_e}{i_0 i_{hj}} \text{ km/h} \quad (17)$$

where, r_b is wheel radius, r_b=0.46m, n_e is engine speed, i_0 is the transmission ratio of main transmission of vehicle, i_0=5.2 and i_{hn} transmission ratio of gearbox, j=1÷5, i_{h1}=3.416, i_{h2}=1.842, i_{h3}=1.290, i_{h4}=0.972, i_{h5}=0.775.

VOL. 16, NO. 23, DECEMBER 2021 ISSN 1819-6608
ARPN Journal of Engineering and Applied Sciences

www.arpnjournals.com

Table-1. Parameters of vehicle and engine.

Parameter	Value	Parameter	Value	Parameter	Value	Parameter	Value
m_1/kg	40	m_e/kg	244	I_{ex}/(kgm^2)	30.7	I_{ey}/(kgm^2)	34.3
m_2/kg	40	m_b/(kg)	1300	I_{bx}/(kgm^2)	800	I_{by}/(kgm^2)	2100
m_3(kg	35	m_4/kg	35	a/m	1.0	b/m	1.56
k_{t1}/(N/m)	2x10^5	c_{t1}/(Ns/m)	0	l_1/m	0.8	l_2/m	0.8
k_{t2}/(N/m)	2x10^5	c_{t2}/(Ns/m)	0	l_3/m	0.8	l_4/m	0.8
k_{t3}/(N/m)	2x10^5	c_{t3}/(Ns/m)	0	x_{b1}/m	1.1	y_{b1}/m	0.74
k_{t4}//(N/m)	2x10^5	c_{t4}//(Ns/m)	0	x_{b2}/m	0.67	y_{b2}/m	0.5
k_1/(N.m^{-1})	98x10^3	c_1/(Ns.m^{-1})	3530	x_{b3}/m	0.78	y_{b3}/m	0.68
k_2/(N.m^{-1})	98x10^3	c_2/(Ns.m^{-1})	3530	x_{e1}/m	0.23	y_{e1}/m	0.08
k_3/(N.m^{-1})	75x10^3	c_3/(Ns.m^{-1})	2860	x_{e2}/m	0.21	y_{e2}/m	0.08
k_4//(N.m^{-1})	75x10^3	c_4//(Ns.m^{-1})	2860	y_{e3}/m	0.11	y_{e3}/m	0.61

Table-2. Parameters of REM and HEM.

Engine mounts	Parameter	Value	Parameter	Value	Parameter	Value
REM	k_{e1}/(N.m^{-1})	225x10^3	k_{e2}/(N.m^{-1})	225x10^3	k_{e3}/(N.m^{-1})	225x10^3
	c_{e1}/(Ns.m^{-1})	98	c_{e3}/(Ns.m^{-1})	98	c_{e3}/(Ns.m^{-1})	98
HEM	k_r/(N.m^{-1})	170x10^3	k_{h1}/(N.m^{-1})	64988	k_{h2}/(N.m^{-1})	656
	c_r/(Ns.m^{-1})	215	c_h/(N.m^{-1})	386	m_{ei} /kg	30.8

From the results of Figure-8, the values of the r.m.s acceleration responses of the vertical motion (awb), pitch and roll angles (awphi and awteta) of vehicle body through Eq. (18), based on the ISO 2631:1997(E) standard, are 0.3158m/s2, 0.3244rad/s2 and 0.4197 rad/s2 respectively for REMs, and are 0.2916 m/s2, 0.2627 rad/s2 and 0.3845 rad/s2, respectively for HEMs. The awb, awphi and awteta values with HEMs respectively reduce by 17.22%, 2.69% and 17.20% in comparison with REMs. The vehicle ride comfort performance of HEMs is significantly improved in comparision with REMs.

$$a_w = \left[\frac{1}{T} \int_0^T a^2(t)dt \right]^{\frac{1}{2}} \tag{17}$$

where, a(t) is the measured or simulated acceleration (translational and rotational) as a function of time, m/s^2 or rad/s^2; T is the duration of the measurement or the simulation time.

In order to continue for the vehicle ride comfort performance evaluation of HEMs in comparison with REMs, the PSD acceleration responses of the vertical motion (a_{PDSb}), pitch and roll angles a_{PSDphi} and $a_{PSDteta}$) of vehicle body consider and analyze when vehicle moves vehicle move on ISO class B surfaces road condition and ICE engine operate at the speed of 1400 rpm (v≈60km/h at i_{h5}=0.775). The a_{PSDb}, a_{PSDphi} and $a_{PSDteta}$ at the speed of 1400 rpm (v≈60km/h at i_{h5}=0.775) are shown Figure-9.

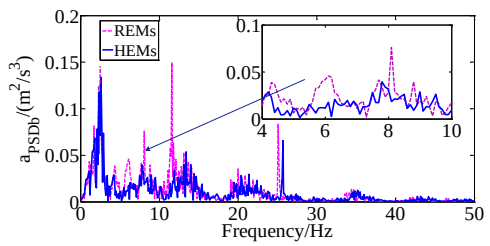

(a) Vertical motion of vehicle body

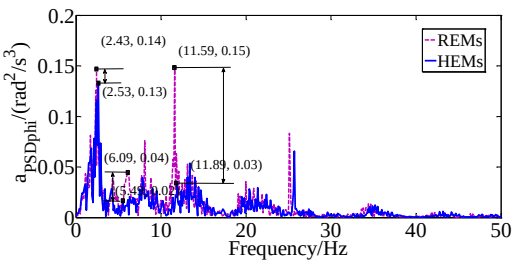

(b) Pitch angle of vehicle body

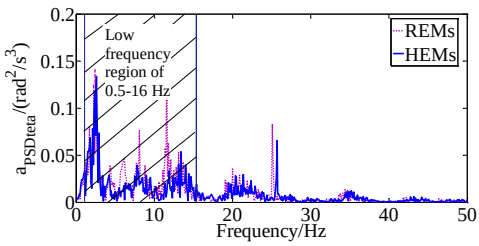

(c) Roll angle of vehicle body

Figure-8. a_{PSDb}, a_{PSDphi} and $a_{PSDteta}$ of vehicle body the speed of 1400 rpm (v≈60km/h at i_{h5}=0.775).

VOL. 16, NO. 23, DECEMBER 2021 ISSN 1819-6608
ARPN Journal of Engineering and Applied Sciences

Figure-9 shows that the peak values of a_{PSDb}, a_{PSDphi} and $a_{PSDteta}$ with HEMs respectively reduce in comparison with REMs. Especially, the peak values of PSD acceleration responses respectively with HEMS at frequencies about 2 Hz, 6Hz and 12 Hz reduce by 7.69%, 100% and 114% in comparison with REMs, which it is greatly reduced in the low frequency region from 0.5Hz to 16Hz. The human body is the most sensitive to vertical vibrations in the frequency range from 4Hz to 10 Hz, lateral and longitudinal vibrations in the frequency range from 2Hz to 4Hz [27, 28]. Vibration in the frequency range from approximately 0.5 Hz to 80 Hz causes discomfort as whole body vibration (WBV), and ISO 2631-1: 1997 standard [27] defines methods of whole-body vibration measurements in the frequency range from 0.5 Hz to 80 Hz for health, comfort and perception and from 0.1Hz to 0.5 Hz for motion sickness. The simulation results indicate that vehicle ride performance of HEMs has done well in reducing those sensitive frequency ranges to the human body in an environment with vibration.

In order to verify the ride comfort performance of HEMs compared to REMs when the vehicle and engine operate under different conditions, the a_{wb}, a_{wphi} and a_{wteta} values change with different road surface conditions and vehicle speed of 60km/h are shown in Figure-9, and the a_{wb}, a_{wphi} and a_{wteta} values change with different vehicle speed conditions and ISO class B surfaces road condition are presented in Table-3. Figure-9 shows that the a_{wb}, a_{wphi} and a_{wteta} values with HEMs respectively reduce in comparison with REMs when the vehicle moves on the different road conditions. That values show that vehicle ride comfort is significantly improved with equipped HEMs for ICE engine in comparison with equipped REMs for ICE engine. In addition, the a_{wb}, a_{wphi} and a_{wteta} values increase very quickly when the road surface condition becomes bad.

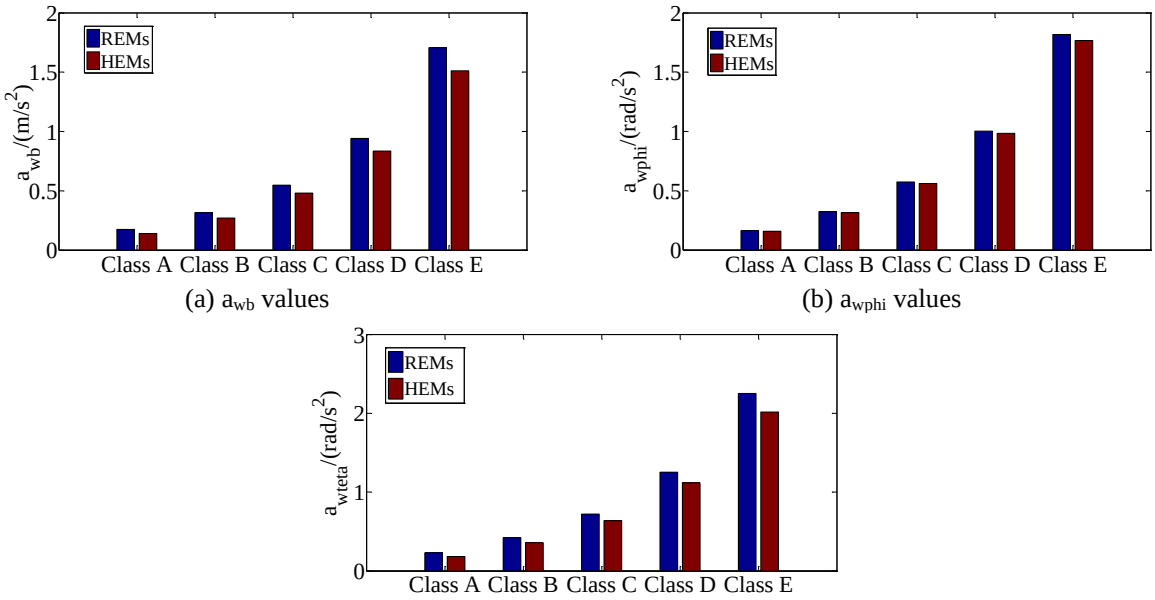

(a) a_{wb} values (b) a_{wphi} values (c) a_{wteta} values

Figure-9. a_{wb}, a_{wphi} and a_{wteta} values change with different road surface conditions and vehicle speed of 60km/h

Table-3. a_{wb}, a_{wphi} and a_{wteta} values change with different vehicle speed conditions and ISO class B surfaces road condition.

n_e rpm/v(km/h) (i_{h5}=0.775)	REMs	HEMs	%	REMs	HEMs	%	REMs	HEMs	%
	a_{wb} (m/s^2)			a_{wphi} (rad/s^2			a_{wteta} (rad/s^2)		
960 /41	0.2447	0.2131	14.83	0.2598	0.2549	1.92	0.3130	0.2682	16.07
1186/51	0.2503	0.2218	12.84	0.2866	0.2717	5.48	0.3441	0.2907	18.37
1420/61	0.3169	0.2766	14.57	0.3285	0.3208	2.40	0.4261	0.3677	15.88
1650/71	0.3611	0.3440	4.97	0.3878	0.3751	3.39	0.4914	0.4229	16.19
1890/81	0.4246	0.4055	4.71	0.4163	0.4125	0.92	0.5139	0.4564	12.59
2120/91	0.4955	0.4559	8.69	0.4406	0.4342	1.47	0.5327	0.4634	14.95
2350/101	0.5487	0.5028	9.13	0.4674	0.4628	3.22	0.5401	0.4698	14.96
2580/111	0.5807	0.5358	8.38	0.4915	0.4838	1.59	0.5329	0.4712	13.09

As seen in Table-3 the awb, awphi and awteta values with HEMs respectively reduce in comparison with REMs when the vehicle moves on the different speed conditions. Those values reveal that the vehicle ride comfort is significantly improved with equipped HEMs for ICE engine in comparison with equipped REMs for ICE engine with the different speed conditions. Especially, the awb, awphi and awteta values with HEMs at vehicle low speed of 51km/h respectively reduce by 12.84%, 5.48% and 18.37% in comparison with REMs. In other words, the hydraulic actuators of HEMs with inertia tracks promote better efficiency in reducing vibration transmitted to vehicle in the low frequency range from 1Hz to 50Hz (n_e<1500prm).

5. CONCLUSIONS

In this study, both the non-linear dynamic model of the hydraulic engine mount (HEM) with inertia track and decoupler and the linear dynamic model of rubber engine mount system are set up to determine the vertical forces. Based on the characteristics of engine mounts, the effects of the vertical linear and nonlinear forces of both REMs and HEMs on vehicle ride comfort are respectively analyzed and evaluated via a full-vehicle dynamic model with the combination of two excitation sources. And then, the vehicle ride comfort performance of HEMs compared with REMs is verified and assessed under different operating conditions of engine and vehicle. The major conclusions drawn from the analysis can be summarized as follows:

a) The a_{wb}, a_{wphi} and a_{wteta} values with HEMs respectively reduce by 17.22%, 2.69% and 17.20% in comparison with REMs when the vehicle moves on ISO class B surfaces road condition and ICE engine operates at the speed of 1400 rpm (v≈60km/h at i_{h5}=0.775).

b) The peak values of PSD acceleration responses with HEMS at frequencies about 2 Hz, 6Hz and 12 Hz reduce respectively by 7.69%, 100% and 114% in comparison with REMs, which it is greatly reduced in the low frequency region from 0.5Hz to 16Hz.

c) The a_{wb}, a_{wphi} and a_{wteta} values with HEMs respectively reduce in comparison with REMs under different operating conditions of engine and vehicle. Especially, the a_{wb}, a_{wphi} and a_{wteta} values with HEMs at vehicle low speed of 51km/h respectively reduce by 12.84%, 5.48% and 18.37% in comparison with REMs.

For future research directions, the authors focus on analyzing and controlling for HEMs with inertia track and decoupler to improve vehicle ride comfort via the full-vehicle dynamic model with the combination of two excitation sources.

ACKNOWLEDGMENTS

This research was supported financially by Thai Nguyen University of Technology, TNUT, Viet Nam.

REFERENCES

[1] Lee J. S. & Kim S. C. 2007. Optimal design of engine mounts rubber considering stiffness and fatigue strength. Proceedings of the Institution of Mechanical Engineers, Part D: Journal of Automobile Engineering. 221(7): 823-835.

[2] Liu C.-H., Chiang Y.-P. & Hsu Y.-Y. 2018. Optimal Design of an Elastomeric Engine Mount with Desired Stiffness using Topology Optimization. 2018 IEEE/ASME International Conference on Advanced Intelligent Mechatronics (AIM).

[3] Zhou H., Liu H., Gao P. & Xiang C.-L. 2018. Optimization Design and Performance Analysis of Vehicle Powertrain Mounting System. Chinese Journal of Mechanical Engineering. 31(1).

[4] Qin H. Y. & Ge X. L. 2011. Design Optimization of Rubber Engine-Mount Based on ANSYS. Applied Mechanics and Materials. 143-144, 480-484.

[5] Azammi A. M. N., Sapuan S. M., Ishak M. R. & Sultan M. T. H. 2018. Conceptual design of automobile engine rubber mounting composite using TRIZ-Morphological chart-analytic network process technique. Defence Technology. 14(4): 268-277.

[6] Seto K., Sawatari K., Nagamatsu A., Ishihama M. & Doi K. 1991. Optimum Design Method for Hydraulic Engine Mounts. SAE Technical Paper Series.

[7] Tikani R., Vahdati N., Ziaei-Rad S. & Esfahanian M. 2010. A new hydraulic engine mounts design without the peak frequency. Journal of Vibration and Control. 17(11): 1644-1656.

[8] Li Q., Zhao J.-C., Zhao B. & Zhu X.-S. 2009. Parameter optimization of a hydraulic engine mount based on a genetic neural network. Proceedings of the Institution of Mechanical Engineers, Part D: Journal of Automobile Engineering. 223(9): 1109-1117.

[9] Christopherson J. & Jazar G. N. 2005. Optimization of Classical Hydraulic Engine Mounts Based on RMS Method. Shock and Vibration. 12(2): 119-147.

[10] Truong T. Q. & Ahn K. K. 2010. A new type of semi-active hydraulic engine mount using controllable area

of inertia track. Journal of Sound and Vibration. 329(3): 247-260.

[11] Mansour H., Arzanpour S., Golnaraghi M. F. & Parameswaran A. M. 2010. Semi-active engine mount design using auxiliary magneto-rheological fluid compliance chamber. Vehicle System Dynamics. 49(3): 449-462.

[12] Hong S.-R. & Choi S.-B. 2005. Vibration Control of a Structural System Using Magneto-Rheological Fluid Mount. Journal of Intelligent Material Systems and Structures. 16(11-12): 931-936.

[13] Hoang A., Le V. *et al* 2019. Influence of damping coefficient into engine rubber mounting system on vehicle ride comfort. Vibroengineering Procedia. 29: 112-118.

[14] Guo R., Gao J., Wei X., Wu Z. & Zhang S. 2017. Full Vehicle Dynamic Modeling for Engine Shake with Hydraulic Engine Mount. SAE Technical Paper Series.

[15] Choi S.-B. S. & Song H.-J. H. 2002. Vibration Control of a Passenger Vehicle Utilizing a Semi-Active ER Engine Mount. Vehicle System Dynamics, 37(3): 193-216. doi:10.1076/vesd.37.3.193.3534.

[16] Hoang Anh Tan, Le Van Quynh, *et al*. 2021. Ride Comfort Analysis of Engine Mounting Systems Using Full Vehicle Dynamic Model, International Journal of Advanced Research in Engineering and Technology (IJARET). 12(1): 448-456.

[17] Colgate J. E., Chang C.-T., Chiou Y.-C., Liu W. K. & Keer L. M. 1995. Modelling of a hydraulic engine mount focusing on response to sinusoidal and composite excitations. Journal of Sound and Vibration. 184(3): 503-528.

[18] Singh R., Kim G. & Ravindra P. V. 1992. Linear analysis of automotive hydro-mechanical mount with emphasis on decoupler characteristics. Journal of Sound and Vibration. 158(2): 219-243.

[19] Lee J. H. & Singh R. 2008. Critical analysis of analogous mechanical models used to describe hydraulic engine mounts. Journal of Sound and Vibration. 311(3-5).

[20] Shangguan W.-B. & Lu Z.-H. 2004. Modelling of a hydraulic engine mount with fluid-structure interaction finite element analysis. Journal of Sound and Vibration. 275(1-2): 193-221.

[21] He S. & Singh, R. 2007. Incorporation of Non-Linear and Quasi-Linear Hydraulic Mount Formulations into a Vehicle Model. SAE Technical Paper Series.

[22] He S. & Singh R. 2005. Estimation of amplitude and frequency dependent parameters of hydraulic engine mount given limited dynamic stiffness measurements. Noise Control Engineering Journal. 53(6): 271.

[23] Geisberger A., Khajepour A. & Golnaraghi F. 2002. Non-Linear Modelling of Hydraulic Mounts: Theory and Experiment. Journal of Sound and Vibration. 249(2): 371-397.

[24] Long L. X., Quynh L. V., Cuong B. V. 2018. Study on the influence of bus suspension parameters on ride comfort. Vibroengineering Procedia. 21: 77-82.

[25] ISO 8608. 1995. Mechanical Vibration-Road Surface Profiles-Reporting of Measured Data. International Organization for Standardization.

[26] Li R., Chen W.-M. & Liao C.-R. 2009. Hierarchical fuzzy control for engine isolation via magnetorheological fluid mounts. Proceedings of the Institution of Mechanical Engineers, Part D: Journal of Automobile Engineering. 224(2): 175-187.

[27] ISO 2631-1. 1997. Mechanical Vibration and Shock-Evaluation of Human Exposure to Whole-Body Vibration, Part I: General Requirements. ISO.

[28] Hassan R. & McManus K. 2002. Perception of Low Frequency Vibrations by Heavy Vehicle Drivers. Journal of Low Frequency Noise, Vibration and Active Control. 21(2): 65-75.